

Imaging of Meningioma Progression by Matrix-Assisted Laser Desorption Ionization Time-of-Flight Mass Spectrometry

Nathalie Y. R. Agar,^{*,†} James G. Malcolm,[‡] Vandana Mohan,[‡] Hong W. Yang,[§] Mark D. Johnson,[§] Allen Tannenbaum,[‡] Jeffrey N. Agar,^{||} and Peter M. Black[§]

Surgical Molecular Imaging Laboratory, Department of Neurosurgery, 221, Longwood Avenue, BLI-137, Brigham and Women's Hospital, Harvard Medical School, Boston, Massachusetts 02115, Schools of Electrical and Computer and Biomedical Engineering, Georgia Institute of Technology, 777 Atlantic Drive NW, Atlanta, Georgia 30332-0250, Neurosurgical Oncology Laboratory, Department of Neurosurgery, 221, Longwood Avenue, EBRC 121, Brigham and Women's Hospital, Harvard Medical School, Boston, Massachusetts 02115, and Department of Chemistry and Volen Center, 415, South Street, Brandeis University, Waltham, Massachusetts 02454

Often considered benign, meningiomas represent 32% of intracranial tumors with three grades of malignancy defined by the World Health Organization (WHO) histology based classification. Malignant meningiomas are associated with less than 2 years median survival. The inability to predict recurrence and progression of meningiomas induces significant anxiety for patients and limits physicians in implementing prophylactic treatment approaches. This report presents an analytical approach to tissue characterization based on matrix-assisted laser desorption ionization time-of-flight (MALDI TOF) mass spectrometry imaging (MSI) which is introduced in an attempt to develop a reference database for predictive classification of brain tumors. This pilot study was designed to evaluate the potential of such an approach and to begin to address limitations of the current methodology. Five recurrent and progressive meningiomas for which surgical specimens were available from the original and progressed grades were selected and tested against nonprogressive high-grade meningiomas, high-grade gliomas, and nontumor brain specimens. The common profiling approach of data acquisition was compared to imaging and revealed significant benefits in spatially resolved acquisition for improved spectral definition. A preliminary classifier based on the support vector machine showed the ability to distinguish meningioma image spectra from the nontumor brain and from gliomas, a different type of brain tumor, and to enable class imaging of surgical tissue. Although the development of classifiers was shown to be sensitive to data preparation parameters such as recalibration and peak picking criteria, it also suggested the potential for maturing into a predictive algorithm if provided with a larger series of well-defined cases.

Meningiomas account for approximately one-third of all primary brain tumors.¹ They develop from the meninges, the tissue

covering the brain and spinal cord, and more specifically are thought to originate from meningotheial cells of the arachnoid membrane, the middle membrane layer of the meninges. The current World Health Organization (WHO) grading system recognizes 15 subtypes of meningiomas based on histological features;² however, these can be classified into three major grades. According to a 10-year retrospective classification of 314 meningiomas, 78% were benign (grade I), 20% atypical (grade II), and 2% malignant (grade III).³ Although meningiomas are often considered benign neoplasms, their recurrence rates vary from 7 to 25% for benign, 29 to 52% for atypical, and 50 to 94% for anaplastic,² the latter being associated with a dismal 1.5 years median survival.⁴ In an attempt to correlate selected immunohistochemical markers with tumor grade and clinical outcome, results indicated that grade and Topoll α index were the only two independent predictive factors of meningioma recurrence.⁵

Since prognosis is intimately related to the appropriateness of treatment modality, it is of paramount importance to identify tumors with high sensitivity and accuracy to maximize treatment efficiency. Unfortunately, some brain tumors are heterogeneous and consist of populations of cells with different degrees of tumor initiating potential^{6,7} and different susceptibility to treatment.^{8,9} These distinct cell subpopulations of tumors can have different proteomes in response to microenvironment conditions and stimuli or as a result of further genetic aberration. Because proteins are dynamic cellular effectors, assessment of their relative concentrations provides valuable information on cellular identity, activity, and state. Proteomic approaches in the search for diagnostic biomarkers involve extensive discovery and validation phases before considering usage approval, and the quest for single marker identification is opening the way to multivariate/multiparametric approaches in response to the complexity of human disease. In addition to the inherent complexity of the disease, the source and

* Corresponding author. Phone: (617) 525-7374. Fax: (617) 264-6316. E-mail: nagar@bwh.harvard.edu.

[†] Surgical Molecular Imaging Laboratory, Department of Neurosurgery, Brigham and Women's Hospital, Harvard Medical School.

[‡] Georgia Institute of Technology.

[§] Neurosurgical Oncology Laboratory, Department of Neurosurgery, Brigham and Women's Hospital, Harvard Medical School.

^{||} Brandeis University.

(1) Central Brain Tumor Registry of the United States (CBTRUS). 2008.

(2) Louis, D. N.; Ohgaki, H.; Wiestler, O. D.; Cavenee, W. K.; Burger, P. C.; Jouvet, A.; Scheithauer, B. W.; Kleihues, P. *Acta Neuropathol.* **2007**, *114*, 97–109.

(3) Willis, J.; Smith, C.; Ironside, J. W.; Erridge, S.; Whittle, I. R.; Everington, D. *Neuropathol. Appl. Neurobiol.* **2005**, *31*, 141–149.

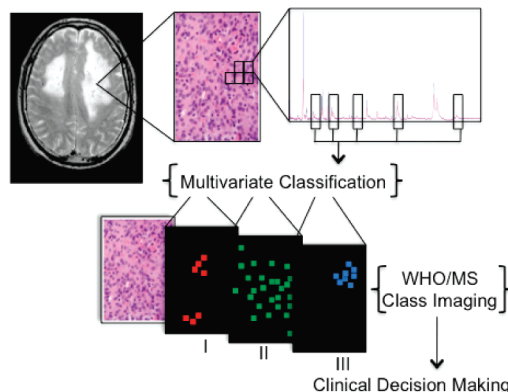
(4) Perry, A.; Scheithauer, B. W.; Stafford, S. L.; Lohse, C. M.; Wollan, P. C. *Cancer* **1999**, *85*, 2046–2056.

(5) Korshunov, A.; Shishkina, L.; Golanov, A. *Int. J. Cancer* **2003**, *104*, 728–734.

complexity of the material selected to identify new diagnostic content in the discovery phase determine the potential of isolating disease markers. The choice of affected tissue for characterization over serum increases detection ability by both an increased concentration of markers to be discovered at the disease site in comparison to dilute circulating markers and sequesters the markers from more abundant constituents of serum which interfere with detection of the less abundant constituents in mass spectrometry.¹⁰

Mass spectrometry (MS) is a well-established analytical technique used to identify and characterize molecules based upon their molecular weight. Matrix-assisted laser desorption/ionization (MALDI) is the ionization method of choice for the MS analysis of large and/or labile biomolecules in complex biological samples.^{11,12} MALDI time-of-flight (TOF) mass spectrometry has developed as a method to evaluate biomolecule expression profiles directly from tissue samples, including brain tumor samples.^{13,14} In mass spectrometry imaging (MSI), hundreds of closely spaced spectra are taken in a grid pattern where each spectrum is analogous to an image pixel.^{15–17} Each pixel contains information on the mass and intensity of hundreds of biomolecules, which can be translated into a spatial map of molecular distribution and abundance.^{18–21} This map can be coregistered to microscopic images to correlate molecular signatures with specific histological features.^{14,22–24} Previous reports of mass spectrometry profiling and imaging of brain tumor tissues have shown differentiation of tumor types, grades, and subclasses of gliomas from large sample sets, and the ability to predict response to treatment by early detection of drug-induced proteomic changes in a breast cancer mouse model.^{13,16,25}

Scheme 1. After a Tissue Biopsy Is Sectioned and Stained, Individual Mass Spectra Are Obtained Uniformly Across a Sister Tissue Section Surface^a



^a Spectra from tissues of different WHO grades are used to perform multivariate classification based on expert histopathology diagnosis. Classification models are then used to grade individual spectra from a tumor specimen, and the molecular images are rendered as class images. From these images, molecular indication of progression could be detected while still not observable by microscopic evaluation and potentially contribute to clinical decision making.

Here, to further adapt mass spectrometry imaging for clinical applications and with the ultimate goal to deliver an objective and accurate evaluation of brain tumor specimens at the time of surgery, human brain tumor samples were analyzed and used to initiate a reference database. This report examines a set of recurrent and progressive meningiomas and presents an approach for building classifiers and addresses potential caveats of data preparation. The clinical concept of mass spectrometry imaging of surgical specimens for prediction of disease progression is illustrated in Scheme 1.

EXPERIMENTAL SECTION

Specimen Selection. Tumor samples were obtained from the Brain Tumor Bank in the Department of Neurosurgery, Brigham and Women’s Hospital (BWH) and analyzed under approved Institutional Review Board (IRB) protocol, with informed written consent obtained by licensed neurosurgeons at BWH. Included in this study are eight patients with histologically proven meningiomas, from which five patients progressed over several years. Many of the patients underwent several surgical tumor resections, each time providing a separate tissue sample for a total of 15 unique meningioma specimens. As control sets, six separate patients provided glioma tumor samples and six separate patients provided nontumor samples (two surgical epilepsy specimens, two postmortem sporadic amyotrophic lateral sclerosis specimens, and two blood samples from healthy individuals).

Materials. “Protein calibration standard 1” from Bruker Daltonics (Billerica, MA) was used for external calibration of the mass spectrometer. Sinapinic acid was from Sigma. ITO coated coverslips with busbars were 18 mm × 18 mm with resistivity from 8–12 Ω (thickness 1, 0.13–0.17 mm) from SPI Supplies (West Chester, PA). ImmEdge PEN was from Vector Laboratories, Inc. (Burlingame, CA).

Sample Preparation for MALDI Mass Spectrometry Imaging. Specimens were sectioned using a Microm HM525 cryostat from Mikron Instruments Inc. (San Marcos, CA) at 16 μm

(6) Singh, S. K.; Clarke, I. D.; Terasaki, M.; Bonn, V. E.; Hawkins, C.; Squire, J.; Dirks, P. B. *Cancer Res.* **2003**, *63*, 5821–5828.
 (7) Singh, S. K.; Hawkins, C.; Clarke, I. D.; Squire, J. A.; Bayani, J.; Hide, T.; Henkelman, R. M.; Cusimano, M. D.; Dirks, P. B. *Nature* **2004**, *432*, 396–401.
 (8) Bao, S.; Wu, Q.; McLendon, R. E.; Hao, Y.; Shi, Q.; Hjelmeland, A. B.; Dewhurst, M. W.; Bigner, D. D.; Rich, J. N. *Nature* **2006**, *444*, 756–760.
 (9) Bao, S.; Wu, Q.; Sathornsumetee, S.; Hao, Y.; Li, Z.; Hjelmeland, A. B.; Shi, Q.; McLendon, R. E.; Bigner, D. D.; Rich, J. N. *Cancer Res.* **2006**, *66*, 7843–7848.
 (10) Zolg, W. *Mol. Cell. Proteomics* **2006**, *5*, 1720–1726.
 (11) Spengler, B.; Kaufmann, R. *Analysis* **1992**, *20*, 91–101.
 (12) Karas, M.; Bachmann, D.; Bahr, U.; Hillenkamp, F. *Int. J. Mass. Spectrom. Ion Processes* **1987**, *78*, 53–68.
 (13) Schwartz, S. A.; Weil, R. J.; Johnson, M. D.; Toms, S. A.; Caprioli, R. M. *Clin. Cancer Res.* **2004**, *10*, 981–987.
 (14) Chaurand, P.; Sanders, M. E.; Jensen, R. A.; Caprioli, R. M. *Am. J. Pathol.* **2004**, *165*, 1057–1068.
 (15) Stoeckli, M.; Chaurand, P.; Hallahan, D. E.; Caprioli, R. M. *Nat. Med.* **2001**, *7*, 493–496.
 (16) Schwartz, S. A.; Weil, R. J.; Thompson, R. C.; Shyr, Y.; Moore, J. H.; Toms, S. A.; Johnson, M. D.; Caprioli, R. M. *Cancer Res.* **2005**, *65*, 7674–7681.
 (17) Seeley, E. H.; Caprioli, R. M. *Proc. Natl. Acad. Sci. U.S.A.* **2008**, *105*, 18126–18131.
 (18) Gusev, A. I.; Vasseur, O. J.; Proctor, A.; Sharkey, A. G.; Hercules, D. M. *Anal. Chem.* **1995**, *67*, 4565–4570.
 (19) Castaing, R.; Slodzian, G. *J. Microsc.* **1962**, *1*, 395–410.
 (20) Stoeckli, M.; Farmer, T. B.; Caprioli, R. M. *J. Am. Soc. Mass Spectrom.* **1999**, *10*, 67–71.
 (21) Caprioli, R. M.; Farmer, T. B.; Gile, J. *Anal. Chem.* **1997**, *69*, 4751–4760.
 (22) Chaurand, P.; Schwartz, S. A.; Billheimer, D.; Xu, B. J.; Crecelius, A.; Caprioli, R. M. *Anal. Chem.* **2004**, *76*, 1145–1155.
 (23) Chaurand, P.; Schwartz, S. A.; Caprioli, R. M. *J. Proteome Res.* **2004**, *3*, 245–252.
 (24) Caldwell, R. L.; Caprioli, R. M. *Mol. Cell. Proteomics* **2005**, *4*, 394–401.
 (25) Reyzer, M. L.; Caldwell, R. L.; Dugger, T. C.; Forbes, J. T.; Ritter, C. A.; Guix, M.; Arteaga, C. L.; Caprioli, R. M. *Cancer Res.* **2004**, *64*, 9093–9100.

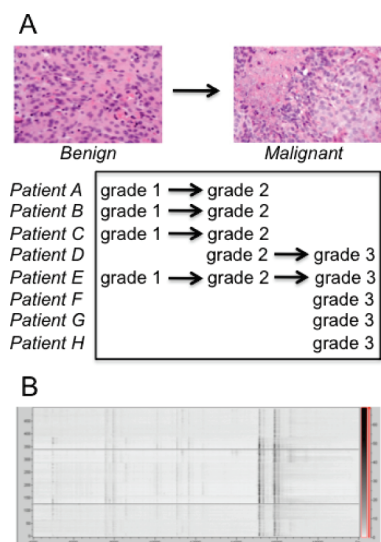


Figure 1. (A) Several cases of meningioma recurred and showed progression in grade; (B) pseudogel view of internally calibrated spectra from MS images used for classification.

thickness. Specimens were prepared by matrix solution fixation.²⁶ Briefly, matrix solution fixation is performed by adding matrix (30 mg/mL final concentration) in a 2:2:1:1 ethanol/methanol/acetonitrile/water 0.2% TFA solution directly to the tissue. A total of 20–40 μ L of matrix solution was deposited and was scaled depending upon the surface area of the sample. After 10 min of fixation at -21 °C, samples were allowed to dry at room temperature.

Mass Spectrometry Profiling and Imaging. A MALDI-TOF mass spectrometer Microflex interfaced with FlexImaging Software, version 2.1, from Bruker Daltonics (Billerica, MA) was operated in linear mode for m/z greater than 3 000 and using a custom-made coverslip holder.²⁶ Standard instrument parameters were used, although delayed extraction times were optimized to between 500 ns for the mass range of interest, 4000–20 000 m/z . The coverslips were held on the target by minimal conductive adhesive tape. Spectral images were acquired at a uniform grid resolution of 100–150 μ m using 300 laser shots at each grid position. Each profile spectrum was generated from 5 000 laser shots spread randomly over the tissue section and summed to create a single spectrum.

Data Analysis. Data were internally calibrated using FlexAnalysis (Bruker Daltonics). Every spectrum underwent manual internal calibration using a two point linear fit to reference masses for singly and double charged hemoglobin. Normalization and classification were performed using ClinProTools, version 2.2 (Bruker Daltonics). The resolution was set at 500 for a mass range of 4 000–20 000 m/z with a top-hat baseline correction of 10%. Unless otherwise noted, peak calculation was driven by a signal-to-noise ratio of 2.0. Peak areas were calculated with the default zero-level integration.

RESULTS AND DISCUSSION

Specimen Selection and Pathology. The selection of specimens as presented in Figure 1A was designed to perform a pilot

study of the mass spectrometry-based classification of human meningiomas, which had clinically progressed. Specifically, specimens were selected from patients who presented for multiple surgeries and with a clear progression from lower to higher grade, thus providing internal controls for comparison. The clinical motivation to perform such a study is to develop a mass spectrometry-based platform to objectively diagnose and potentially provide predictive indicators of tumor recurrence and progression for meningioma patients. Two neuropathologists independently graded the specimens with no interobserver variability, and the concept of using matching specimens from one patient should minimize variability arising from individuals' molecular profiles within the series.

Increasing the Resolution of Molecular Profile Mass Spectra with Imaging. This study analyzes and classifies samples at two different levels. First, a single high signal/noise "profile" spectrum representing the entire tissue is generated by signal averaging thousands of spectra acquired across the surface of the tissue, without preserving spatial distribution information. This experiment is analogous to the widely used "molecular profile" experiments performed on various tissue samples using MALDI- and surface-enhanced laser desorption ionization (SELDI)-TOF platforms.^{14,27} Second, a mass spectral image was generated using hundreds to thousands of lower signal/noise spectra (because only \sim 300 spectra could be acquired at a given location before exhausting signal production) acquired in a grid pattern across the surface of the tissue.

In the course of optimizing instrument parameters, location-dependent peak shifting was observed (e.g., hemoglobin mass measured as 15 119 m/z at one position and 15 245 m/z at another). Thus, a given peak from a profile spectrum created by averaging spectra from different locations is the convolution of peaks with different maxima. Such profile spectra, generated by randomly collecting spectra from a tissue's surface were characterized by peak broadening, decreased resolution, and appearance of possible artifact peaks. These problems were overcome by averaging internally calibrated spectra from mass spectral images, which resulted in resolution (full width at half height, fwhh) increases of 1.2 ± 0.3 -fold for evaluated peaks ranging from 5 000 to 15 200 m/z . The effect was also more significant (e.g., 1.6) on peaks of higher intensities, whereas low-intensity peaks showed a slight increase in resolution from profiling. Such internal calibration using the singly and doubly charged forms of hemoglobin had the added benefit of minimizing data classification errors, since the maximum allowed peak shift for recalibration in ClinProTools (2000 ppm) was significantly less than the experimental variance in molecular mass (\sim 5000 ppm). Thus, spectra that were not internally calibrated resulted in the improper binning of peaks (features) such that the peak that was actually hemoglobin was mistaken for two different molecules during classification, creating artifactual differences between two samples. The pseudogel view in Figure 1B shows the resulting quality of alignment from manual recalibration of 500 image spectra.

Classification and Prediction of Progression. The realigned spectra from 15 images were subjected to Principal Component Analysis (PCA) resulting in the apparent unsupervised segregation

(26) Agar, N. Y.; Yang, H. W.; Carroll, R. S.; Black, P. M.; Agar, J. N. *Anal. Chem.* **2007**, *79*, 7416–7423.

(27) Whelan, L. C.; Power, K. A.; McDowell, D. T.; Kennedy, J.; Gallagher, W. M. *J. Cell. Mol. Med.* **2008**, *12*, 1535–1547.

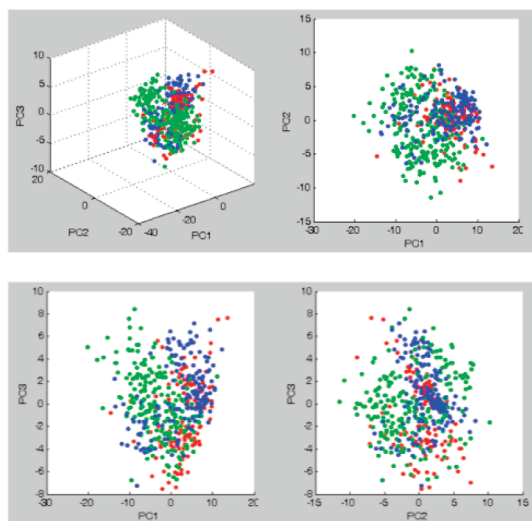


Figure 2. Principal component analysis using peak intensities indicates the potential for automatic grading via cluster analysis: grade I (red), grade II (green), and grade III (blue).

g + m 98%	ntb 2%	
m 96%	ntb 4%	
m 93%	g 6%	ntb 1%

Figure 3. General classification of meningioma images using a support vector machine trained on graded profiles. Combined with a nontumor training set, several tumor sets were examined: meningiomas combined with gliomas, only meningiomas, and meningiomas and gliomas separately. The ability to generally distinguish tumor from nontumor under each scenario indicates the potential of this approach in a clinical setting. Labels indicate nontumor brain (ntb), meningioma (m), and glioma (g) and percentages represent the distribution of total meningioma image spectra recognized by a given class.

of each grade in accordance to histopathological grade (Figure 2). Support vector machine (SVM) classification models constructed using profile and image spectra suggested to be capable of recognizing image spectra of meningiomas using classifiers built from (1) a single brain tumor class that compared both glioma and meningioma with nontumor tissue (including blood); (2) a meningioma brain tumor class and nontumor brain class; and (3) a meningioma class, a glioma class, and a nontumor brain class (Figure 3). Including blood specimens in the control group minimizes its contribution to signals derived from surgical tumor specimens, which can be infiltrated and/or retain blood from bleeding in the surgical cavity. Training sets were built using the current gold standard of WHO histopathology classification of tumors of the central nervous system. Although sampling needs to be significantly increased to propose a predictive multivariate indicator of progression, the concept begins to emerge from the

Table 1. Classification of Imaged Biopsies^a

histological	WHO grade								
	I			II			III		
	% spectra								
MSI									
A				83	1		26	9	65
B	42	50	8	43	29	28			
B ^{*b}		30	70						
C		50	50	10	18	72			
patients	D			12	18	70	2	37	58
E		10	90		4	92	2		98
F									100
G									100
H							15	11	74
total	4	24	72	26	20	54	8	10	82

^a Imaged biopsies were manually and automatically graded. Each biopsy is reported within the column indicating its histological WHO classification. Within this group, the MSI classifier reports the percent of image classified according to each grade. ^b B* represents a specimen from patient B with nonprogressive recurrence.

results presented in Table 1. The percentage distributions between the three grades were more pronounced in samples A–E, while F–H (which did not present with a history of recurrence and progression) showed more segregation to their histological grade.

It is also of interest to understand the contribution of interindividual variance in discriminating between different tumor grades, since the data set does not include all three grades imaged for each subject. Toward this goal, the seven peaks used by the SVM for classification were plotted as a box-and-whisker plot from all grades over all the subjects (Figure 4A) and compared to the equivalent plot for the same seven classifying peaks for one subject (Figure 4B). The discrimination ability of the peaks is comparable between the two plots, suggesting an intergrade variance rather than an interindividual variance. While future increased sampling should increase the robustness of these findings, the box-and-whisker plots indicate a classification dominated by intergrade variance, with minimal interindividual variance contribution, justifying further development of the framework for molecular diagnosis. In the identification of a novel serum tumor marker for colorectal cancer using a classical proteomic approach, a group from Roche Diagnostics reported the use of 16-matched colorectal cancer spanning the 4 Dukes stages and adjacent normal tissue samples for the initial discovery phase.^{10,28} While it is not possible to retain matched-healthy tissue from the brain, the use of matched recurrence specimens minimizes interindividual contribution. When combined with control groups constituted of distinct types of brain tumor and independent nontumor tissues, this approach provides with a valid initial reference frame.

This phenomenon and perceived advantage of imaging the specimens in comparison to profiling is represented in Figure 5. This presents the class imaging results of a grade II specimen (selected region of analysis) from subject E, who presented with tumor recurrence and a progression to grade III. The advantages of preserving spatial resolution in the mass spectrometry analysis of surgical specimens include not only higher resolution spectra

(28) Roessler, M.; Rollinger, W.; Palme, S.; Hagmann, M. L.; Berndt, P.; Engel, A. M.; Schneidinger, B.; Pfeffer, M.; Andres, H.; Karl, J.; Bodenmuller, H.; Ruschoff, J.; Henkel, T.; Rohr, G.; Rossol, S.; Rosch, W.; Langen, H.; Zolg, W.; Tacke, M. *Clin. Cancer Res.* **2005**, *11*, 6550–6557.

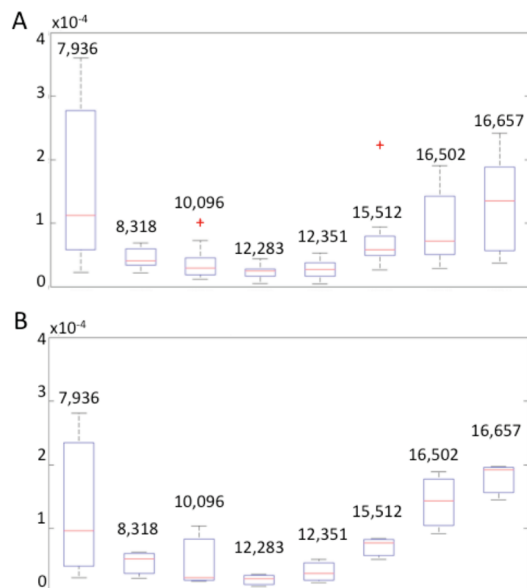


Figure 4. Box-and-whisker plot statistical representation of peaks used by the SVM classifier: (A) discrimination ability of the SVM peaks from the complete data set including all available subjects, for all tumor grades; (B) box-and-whisker plot of spectra from data set for one randomly selected subject, for all tumor grades. Discrimination ability of the SVM peaks for a selected subject's data set including all tumor grades. The lower and upper quartiles in each box are delineated by the median represented by a red line; the smallest and largest observations are indicated by corresponding whiskers; red crosses outside the whiskers delimited regions report outliers.

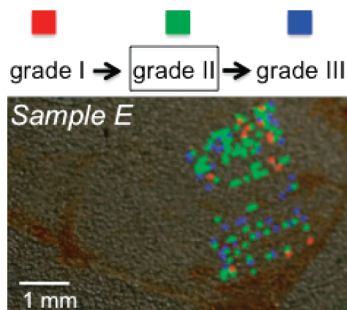


Figure 5. Class imaging of a tissue specimen of histological grade II from a patient with progressive recurrence from grade I to II and to III shows the presence of regions of distinct grades. While many image spectra were discarded as null or noisy, the admissible spectra suggest spatial clustering of the different grade signals. Colored pixels represent grade I (red), grade II (green), and grade III (blue) regions.

but also the ability to detect these spectra with an underlying character of higher grade otherwise not recognizable by standard histopathological evaluation. Taken together with clinical presentation, radiology findings, and standard histopathology evaluation, MSI, once validated with larger sample sets, could contribute to clinical decision-making. Unraveling the grade of a tumor by its molecular characterization could provide access to treatment protocols otherwise not available for a standard histopathology grade and potentially decrease recurrence probability.

Although such results are encouraging in developing approaches to assist in the management of neurosurgical diseases, the preparation of the data to build classifiers has a profound effect upon the results of classification and thus one must be very careful in the interpretation of the results. The sensitivity of the overall

Table 2. Effect of Peak Selection Signal to Noise Ratio (S/N) on Classification^a

S/N	peaks	% spectra								
		I			II			III		
		I	II	III	I	II	III	I	II	III
1	6	2	37	60	19	23	58	6	15	79
2	5	4	23	73	27	20	53	8	10	82
4	8	3	13	84	25	7	68	9	8	83
6	2	2	2	95	12	12	76	6	6	89

^a Classification is sensitive to the signal-to-noise ratio used in selecting peaks. The experiment in Table 1 was repeated under various ratios to illustrate the effect on number of peaks used in the classifier and subsequent totaled classification represented in percentages of total image spectra classified within each MSI class.

analysis to data preparation implies that further development of more robust data preprocessing and classification is required. Classification results for the total number of image spectra for each grade is presented in Table 2 for S/N criteria ranging from 1 to 6 and justify the further development and automation of appropriate data preprocessing applications to streamline the preparation of large numbers of spectra for classification. Further, while the support vector machine technique seemed to work well for our purposes, a neural network approach for the data classification will be tested as well as the relevance vector machine (RVM) technique. The RVM classification method is a Bayesian extension of SVM, which achieves comparable performance to SVM while providing posterior probabilities for class memberships and a sparser model. Clustering may also be improved using a kernel PCA methodology in which one does not need to assume linear models.

CONCLUSIONS

A comprehensive molecular diagnosis obtained during surgery would enable physicians to tailor treatment by accurate evaluation of tumor type and grade and to select the best suited treatment regimen on an individual basis. MALDI MSI is an approach with potential in image-guided therapy, and its incremental validation will be driven by the inclusion of large and diversified arrays of tumor specimens. Moreover, the diversity of a well-documented database including detailed clinical information will later allow more refined predictive models for personalized cancer management.

ACKNOWLEDGMENT

We thank Dr. Jennifer Chan for the pathology assessment. We thank Bruker Daltonics and its employees for continued collaboration. We thank Jane-Marie Kowalski and Paul Kowalski for their continued technical assistance. This research was funded by grants from the Brain Science Foundation and the American Brain Tumor Association (ABTA) and support from the Daniel E. Ponton Fund for the Neurosciences to N.Y.R.A. and supported in part by awards from the DOD (Contract W81XWH-04-0158) and the ALS Association to J.N.A. This work was also supported in part by NIH Grants NAC P41 RR-13218 and NAMIC U54 EB005149 through Brigham and Women's Hospital.

Received for review January 14, 2010. Accepted February 24, 2010.

AC100113W